Supplementary Information for

Stretchable sensor platform based on simple and scalable lift-off micropatterning of metal nanowire network

Dong-Wook Jeong,[a] Nam-Su Jang,[a] Kang Hyun Kim,[a] and Jong-Man Kim*[a,b]

[a] Department of Nano Fusion Technology and BK21 Plus Nano Convergence Technology Division, Pusan National University, Busan 46214, Republic of Korea.
[b] Department of Nanoenergy Engineering, Pusan National University, Busan 46214, Republic of Korea. *E-mail: jongkim@pusan.ac.kr

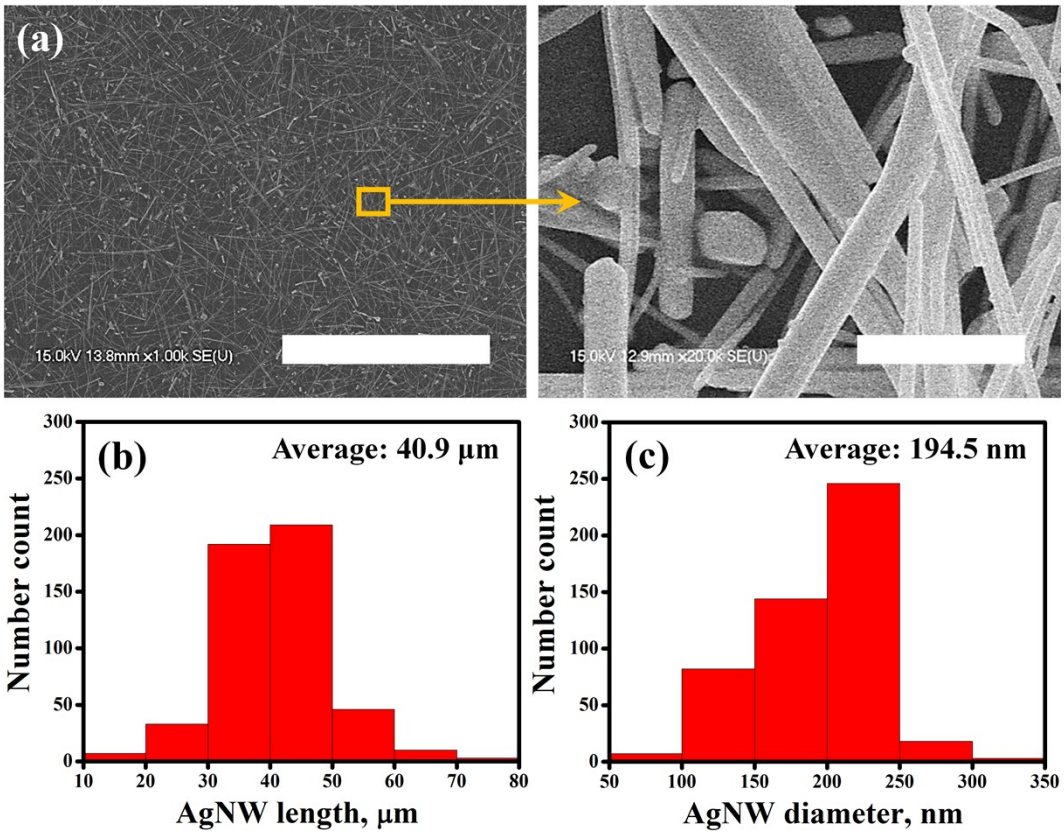

Fig. S1 AgNW synthesis. (a) SEM images of AgNWs synthesized using a modified polyol process (scale bars: 200 µm (left), 2 µm (right)), and histograms of (b) length distribution and (d) diameter distribution (500 AgNWs measured).

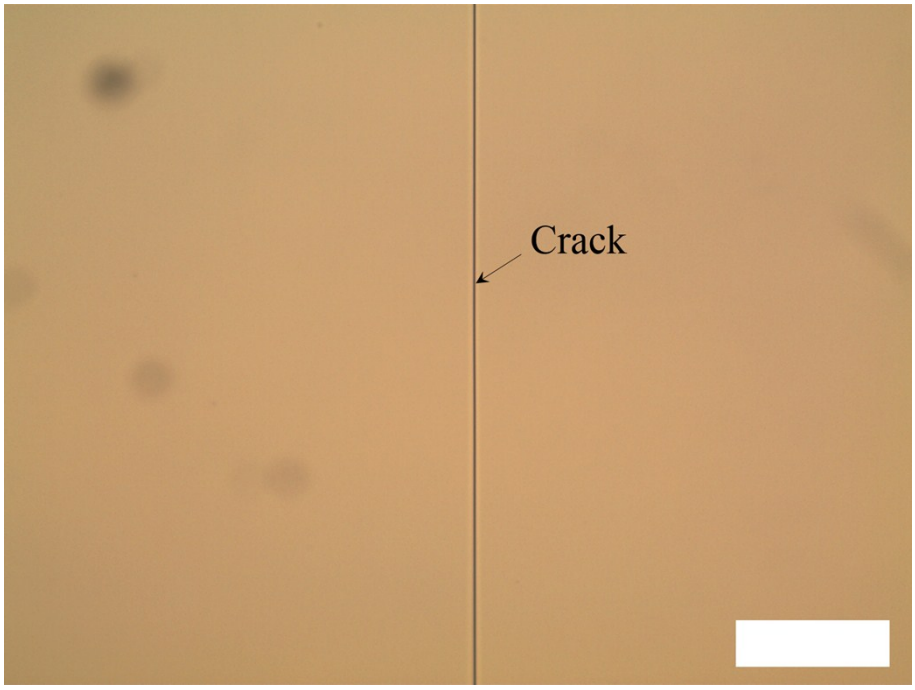

Fig. S2 Microscope image of crack typically generated on the PR layer (scale bar: 50 μm).

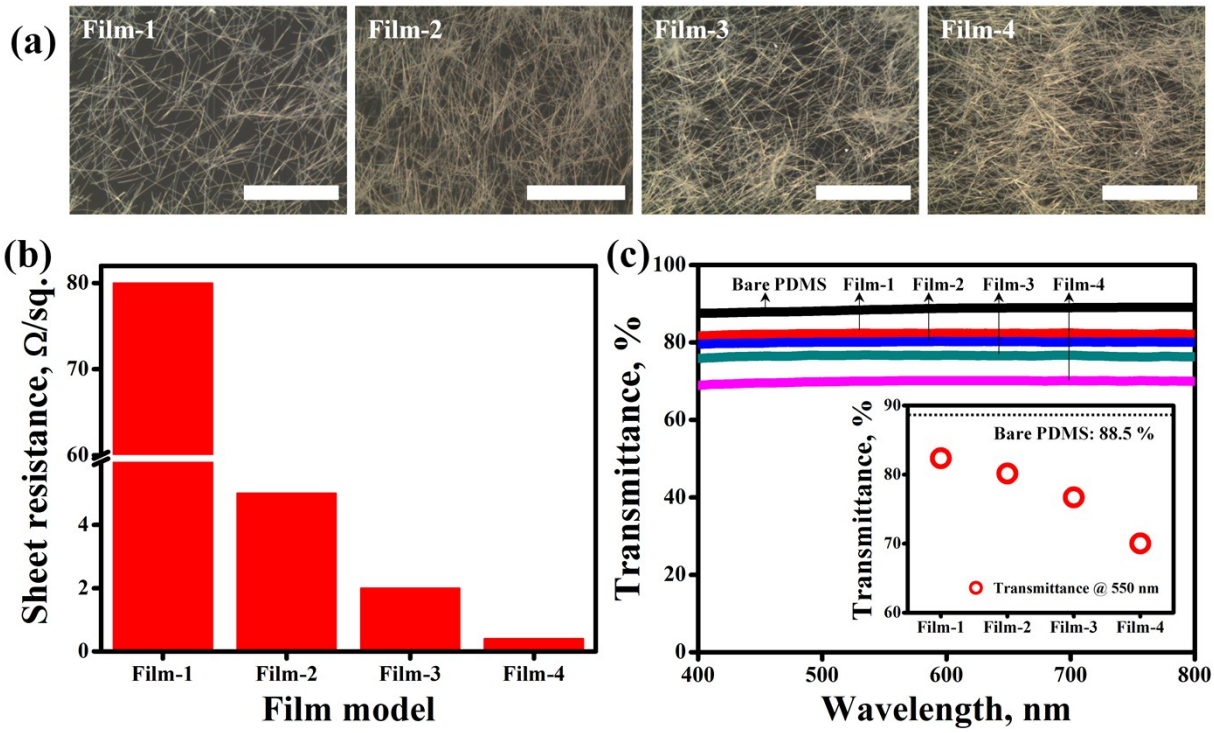

Fig. S3 Electrical and optical properties of AgNW films prepared by spray coating AgNWs on PDMS substrate with different coating volume (Film-1: 5 mL, Film-2: 10 mL, Film-3: 15 mL, and Film-4: 20 mL) with respect to fixed concentration of AgNW solution (20 mg/mL). (a) digital images (scale bars: 50 μm), (b) sheet resistances and (c) optical transmittances (inset: transmittance @ 550 nm) of each AgNW film.

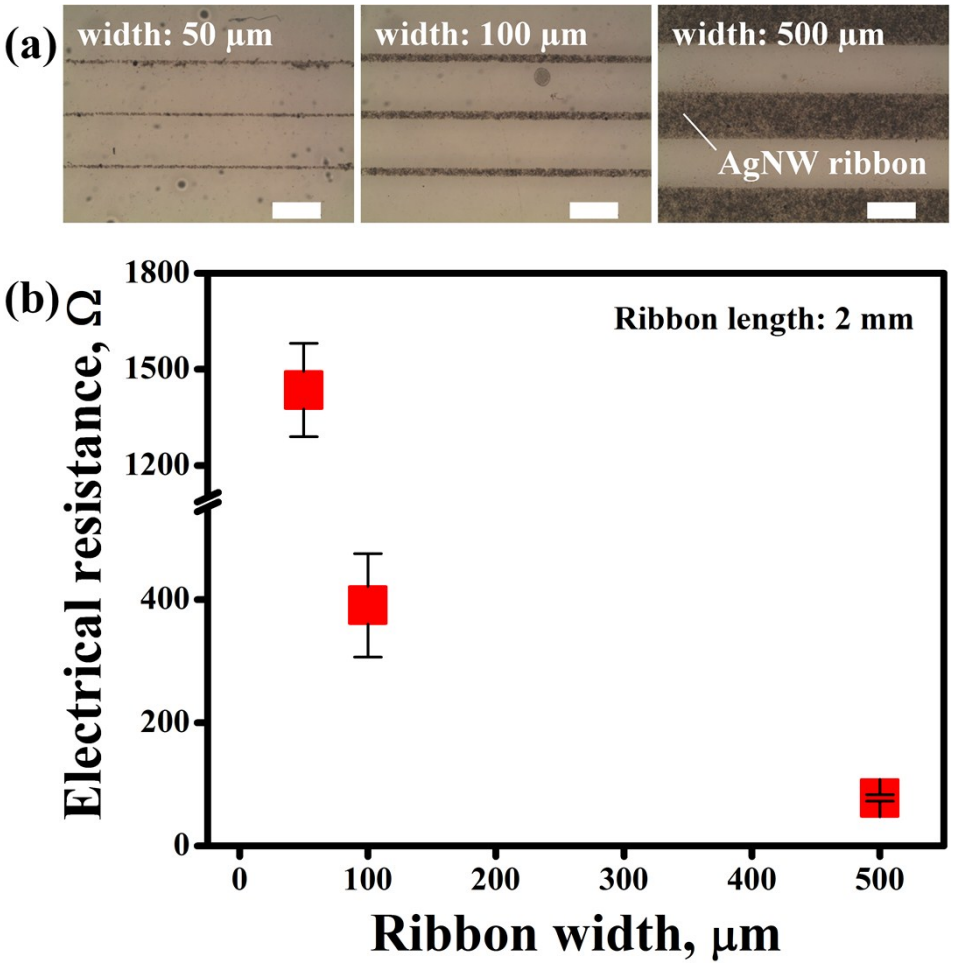

Fig. S4 AgNW percolation network ribbons with different widths (50, 100, and 500 μm) and fixed length (2 mm). (a) OM images (scale bars: 500 μm) and (b) electrical resistance of each ribbon.

Electrical resistance (R) of a conductor is determined by $R = \rho(l/A) = \rho(l/wt)$ where ρ is the resistivity, l, w, and t are the length, width, and thickness of the conductor, respectively. In the geometrical point of view, R is directly proportional to l and inversely proportional to the cross-section area ($A = w \times t$). Therefore, R of the AgNW ribbon is exponentially decreased with increasing w because only w is increased with respect to the fixed ρ, l, and t of the ribbon. However, it was found that decrease in the electrical resistance of the AgNW ribbon is faster than the width-dependent change. This is probably because larger AgNW ribbons can be more precisely defined while the patterning uncertainty is minimized, compared to the smaller ones. In addition to this, uniformity of AgNW percolation network on the ribbon would be also an influential factor that causes the variation in the electrical resistance of the ribbons.

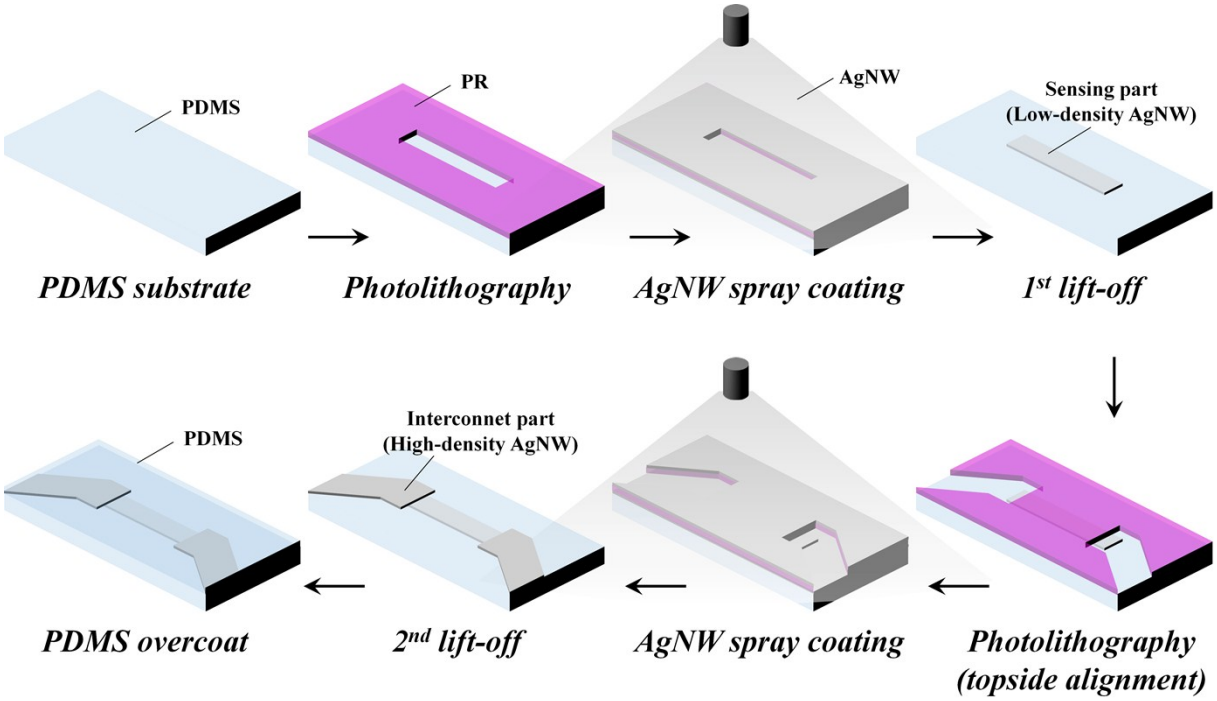

Fig. S5 Schematic illustration of fabrication sequence of stretchable resistive strain sensor based on the TMA-based lift-off micropatterning process of AgNWs. The sensing part (low-density AgNW network) is formed on a PDMS substrate using the first lift-off, and the horseshoe-shaped stretchable interconnects (high-density AgNW network) are formed using the second lift-off after aligning the second photomask precisely to the prepatterned sensing part.

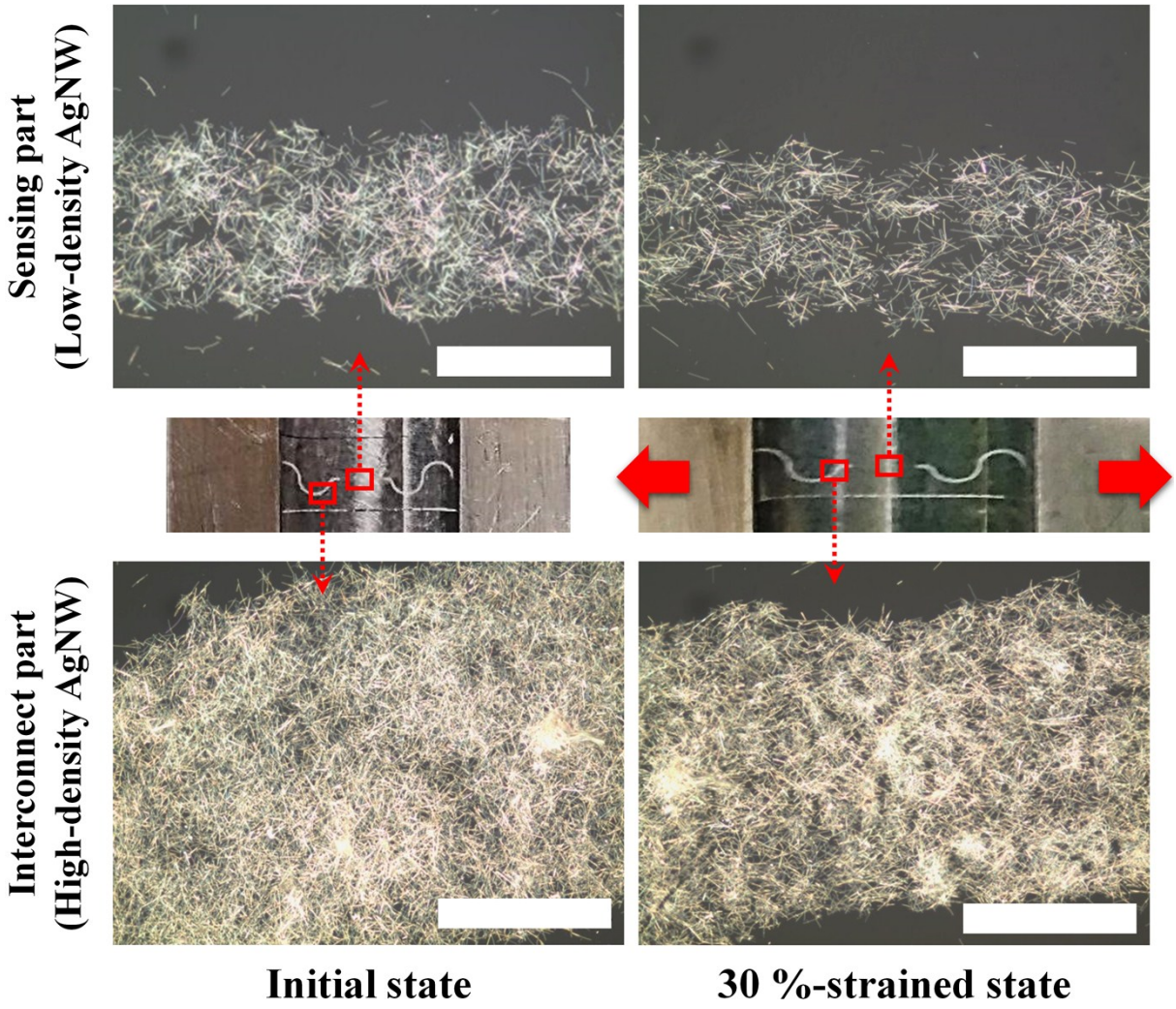

Fig. S6 Digital and OM images of the sensing and interconnect parts of the stretchable resistive strain sensor strain under the initial and 30 %-stretched states (scale bars: 100 μm).

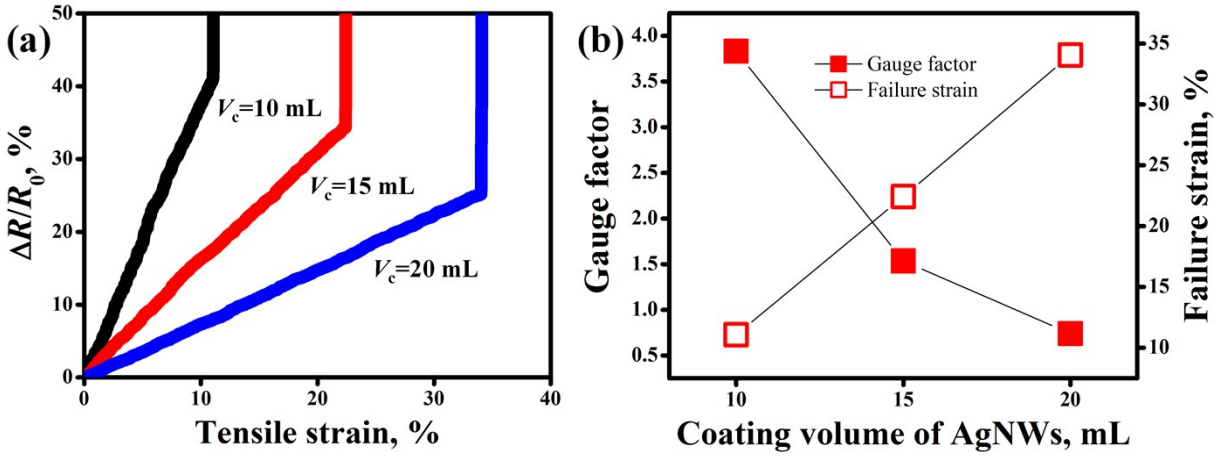

Fig. S7 Sensing performance of stretchable resistive strain sensor according to coating volume of AgNWs (V_c = 10, 15, 20 mL) at the sensing part with respect to fixed concentration of AgNW solution (20 mg/mL). (a) $\Delta R/R_0$ of the devices in response to tensile strain at a loading speed of 0.4 mm/sec (5 %/sec), and (b) gauge factors and failure strains of each device with different AgNW density in the sensing part.

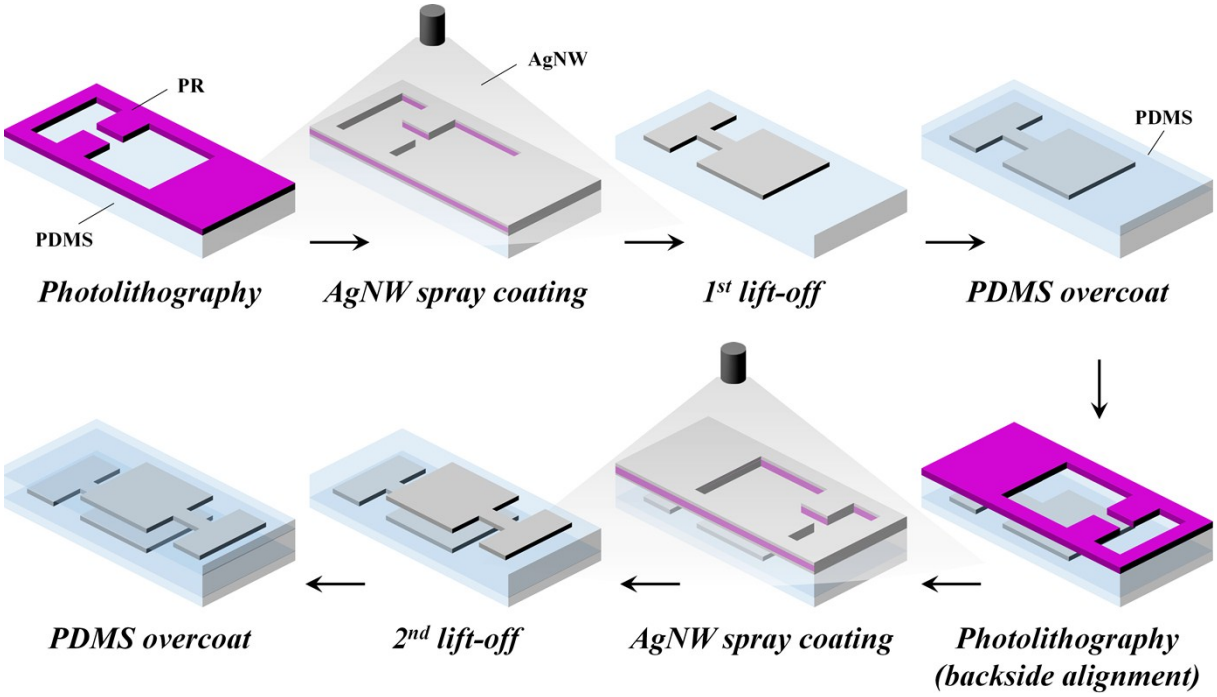

Fig. S8 Schematic illustration of fabrication sequence of elastic capacitive pressure sensor based on the BMA-based lift-off micropatterning process of AgNWs. The top electrode is formed on a PDMS substrate using the first lift-off, and the bottom electrode is formed on the opposite side of the substrate using the second lift-off after aligning the second photomask precisely to the prepatterned top electrode that is seen through the transparent PDMS substrate.

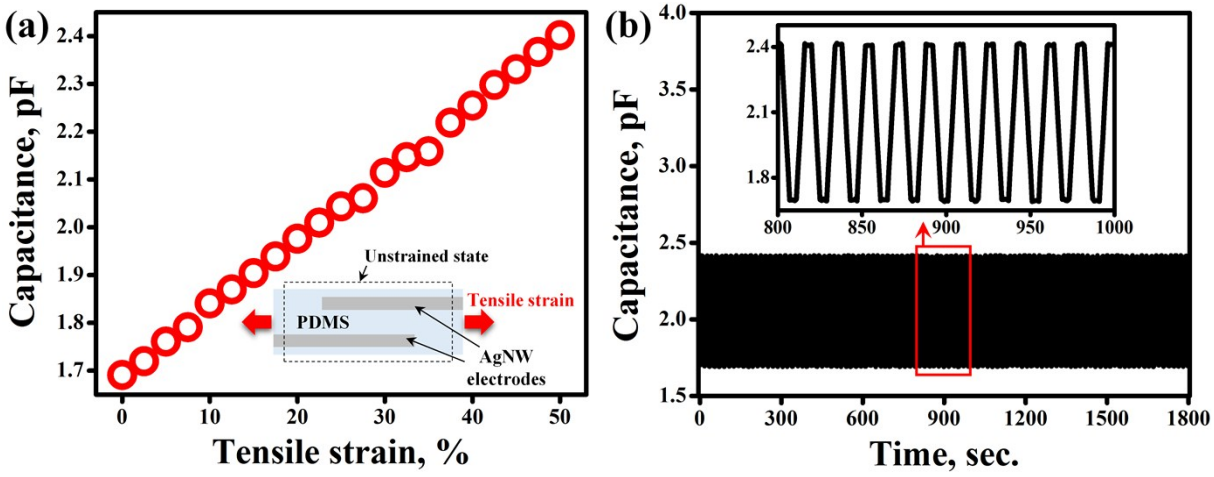

Fig. S9 Elastic capacitive pressure sensor under stretching deformation. Change in the capacitance of the sensor (a) in response to tensile strain for up to 50 % at a loading speed of 0.1 mm/sec (5 %/sec) (inset: schematic illustration of the sensor under stretching), and (b) under repetitive stretching for up to 100 cycles with a maximum tensile strain of 50 % at a loading speed of 0.2 mm/sec (10 %/sec) (inset: magnified profile of capacitance change for 10 cycles).

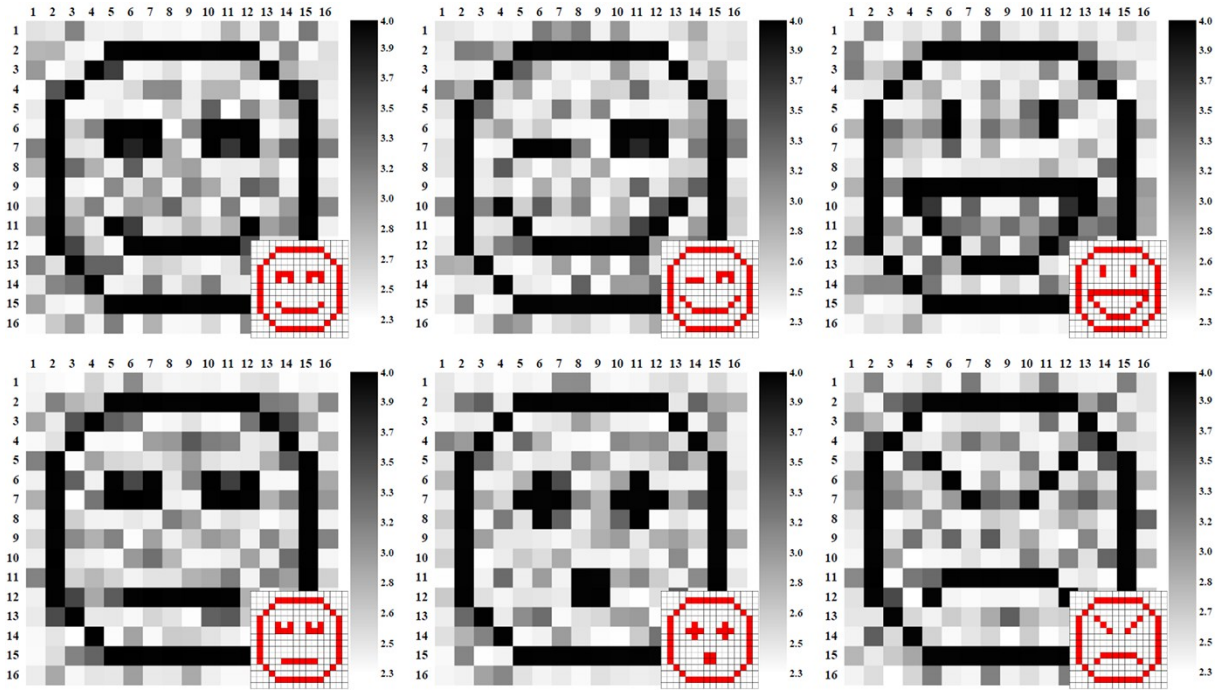

Fig. S10 Image plots of various facial expressions obtained from the 16 × 16 pressure sensor array (inset: schematic illustrations of force maps on the sensor array; Red parts indicate the forced regions.).